

Inclined-Field Structure, Morphology, and Pinning of the Vortex Lattice in Microtwinned $\text{YBa}_2\text{Cu}_3\text{O}_7$

B. Keimer,* F. Doğan, I. A. Aksay, R. W. Erwin, J. W. Lynn, M. Sarikaya

A detailed small-angle neutron scattering study of the vortex lattice in a single crystal of $\text{YBa}_2\text{Cu}_3\text{O}_7$ was made for a field of 0.5 tesla inclined at angles between 0 and 80 degrees to the crystalline c axis. The vortex lattice is triangular for all angles, and for angles less than or equal to 70 degrees its orientation adjusts itself to maximize the pinning energy to densely and highly regularly spaced twin planes. These observations have important implications for the microscopic flux-pinning mechanism, and hence for the critical current achievable in $\text{YBa}_2\text{Cu}_3\text{O}_7$. For large angles (about 80 degrees) the vortex lattice consists of independent chains in the orientation predicted by anisotropic London theory.

The nature of the vortex state in the cuprate high-temperature superconductors remains an issue of great theoretical and practical interest. A variety of experimental techniques have been used to investigate the static and dynamic vortex correlations in these materials. In contrast to surface imaging techniques, such as low-field ($B \leq 0.005$ T) Bitter decoration (1) or scanning tunneling microscopy (2), neutron scattering is sensitive to the entire length of the vortices in the bulk of the material. Neutron scattering experiments can be performed in a magnetic field range of ~ 0.05 T up to several teslas, a theoretically interesting regime in which the vortices interact strongly. This is also the relevant field range for prospective magnet applications of the copper oxide superconductors. In fact, the success of our experiments depended critically on the preparation of a large (~ 2.5 -cm diameter, 0.9-cm thickness), high-quality single crystal in a program devoted to device applications of bulk $\text{YBa}_2\text{Cu}_3\text{O}_7$.

The experiments address two interrelated issues. First, the layered structure of the copper oxides and the concomitant large anisotropy of the electronic properties give rise to complex current and field distributions around individual vortices. The ensuing unusual interactions between vortices can lead to novel vortex structures as the magnetic field is inclined at an angle θ with respect to the c axis (1). By performing neutron experiments for $0^\circ \leq \theta \leq 80^\circ$, we tested these theories in fields up to 0.5 T.

A second issue of great practical signifi-

cance is the interaction of the vortex lattice with pinning centers that prevent dissipative vortex motion at high temperatures and cause flux trapping as the external field is removed. We carried out extensive electron microscopy studies to identify the microstructural features potentially responsible for flux pinning in our samples. Our neutron measurements indicate that among the possible candidates (inclusions of the nonsuperconducting Y_2BaCuO_5 phase, stacking faults, and twin planes) only the densely spaced twin planes have a substantial effect on the structure of the vortex lattice. Prior evidence for the importance of twin planes as pinning sites derives mainly from Bitter decoration (3) and transport (4) studies conducted for either $\theta = 0^\circ$ or $\theta = 90^\circ$. We show that the vortex lattice orientation locks into the orientation of the twin planes up to a surprisingly large inclination angle $\theta \approx 70^\circ$. We discuss this observation in terms of microscopic models of the vortex structure. For larger inclination angles, we report

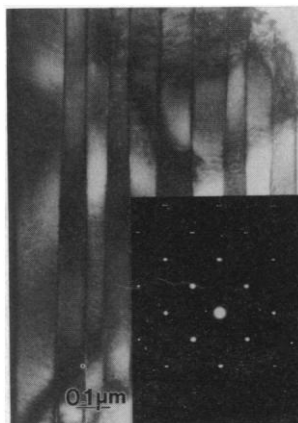


Fig. 1. Electron micrograph showing one family of twin boundaries in our $\text{YBa}_2\text{Cu}_3\text{O}_7$ crystal. The inset is a selected-area diffraction pattern (20- μm aperture) with the electron beam in the [001] direction, showing the orthorhombic splitting of the reflections.

the observation of a vortex chain state.

The single-crystal sample was synthesized by a seeding technique in a temperature gradient (5). The characterization of our sample by transmission electron microscopy was carried out by the cutting of several sections perpendicular to the (001) and (110) planes from an identically prepared crystal. A selected-area diffraction pattern with the electron beam in the [001] direction is shown in the inset in Fig. 1. The orthorhombic strain $\Delta a = (b_0 - a_0)/a_T = 1.8\%$ (a_0 , b_0 , and a_T are the basal-plane lattice parameters in the orthorhombic and tetragonal phases) determined from the splitting of the [110] diffraction peak is identical for several sections of the sample, which proves that oxygen is distributed homogeneously throughout the bulk of the sample. The strain created as the sample is cooled through the tetragonal-orthorhombic transition at 700°C is relieved by the formation of two variants of twin boundaries on the (110) and ($1\bar{1}0$) planes (Fig. 1). As discussed previously (6), the separation D of the twin boundaries is inversely proportional to Δa , so the highly regular twin-plane spacing again indicates a homogeneous distribution of oxygen. By measuring 250 twin domains, we obtained $D = 900 \pm 30$ Å. We determined the width of the twin boundaries to be 15 ± 5 Å from the width of the weak rod of scattering extending in the [$1\bar{1}0$] direction outside the [110] diffraction peak of Fig. 1. Because this width is of the order of the in-plane superconducting coherence length, the twin planes may be effective core-pinning sites.

Our coordinate system is defined in Fig. 2 (7). The angles χ and ϕ are determined by the orientation of the crystal by x-ray diffraction outside the cryostat. Once the sample is mounted in the cryostat, the angles θ and ϑ can be changed by the rotation of either the cryostat inside the magnet or the entire cryostat-magnet assembly, respectively. The crystalline (100) axis was kept in the (\hat{x} , \hat{y})

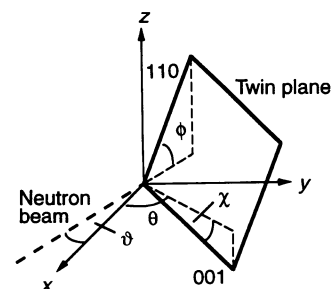


Fig. 2. Coordinate system defining our angle conventions. Our experiments were carried out with χ fixed at either 0° or 9° , ϕ fixed at 45° , and θ and ϑ varied. The coordinates \hat{y} and \hat{z} perpendicular to the magnetic field (x axis) are the abscissa and ordinate, respectively, in the diffraction patterns of Fig. 3.

B. Keimer, Department of Physics and Princeton Materials Institute, Princeton University, Princeton, NJ 08544.

F. Doğan and I. A. Aksay, Department of Chemical Engineering and Princeton Materials Institute, Princeton University, Princeton, NJ 08544.

R. W. Erwin and J. W. Lynn, National Institute of Standards and Technology, Gaithersburg, MD 20899.

M. Sarikaya, Princeton Materials Institute, Princeton University, Princeton, NJ 08544, and Department of Materials Science and Engineering, University of Washington, Seattle, WA 98195.

*To whom correspondence should be addressed.

plane to $\pm 3^\circ$, so that $\phi \approx 45^\circ$. We performed the neutron scattering experiments for two different values of χ : $0^\circ \pm 1^\circ$ and $9^\circ \pm 1^\circ$. It is important to understand the difference between these two configurations: In the first case ($\chi = 0^\circ$), the magnetic field bisects the angle between the two sets of twin planes for any value of θ . In the second case, the c axis is slightly offset from the field direction by $\chi = 9^\circ$ at $\theta = 0^\circ$, so that for $\theta \neq 0^\circ$ the angles α_\pm subtended between the magnetic field and the two sets of twin planes are different: $\alpha_\pm = \sin^{-1}[(\sin \theta \pm \cos \theta \sin \chi)/\sqrt{2}]$. This small difference in angle has profound consequences for the structure of the vortex lattice.

The data for $\chi = 0^\circ$ and $\chi = 9^\circ$ are shown in Fig. 3, A to F, and Fig. 3, G to I, respectively. For $\theta = \chi = 0^\circ$, we observe the diffraction pattern with fourfold symmetry reported for both zero and nonzero θ (8, 9). This result led Yethiraj and co-workers (9) to the conclusion that the vortices form a square lattice, which maximizes the binding energy between vortices and both sets of twin planes, rather than the triangular lattice expected if vortex-vortex interactions dominate. To investigate this point further, we oriented the crystal so that $\chi = 9^\circ$ and $\theta = 5^\circ$ (Fig. 3G). This small angular offset causes a single-domain triangular lattice to be formed in the entire crystal, as evidenced by the hexagonal diffraction pattern. A fit to the circularly averaged intensity profile gave a peak position (τ) of $0.0092 \pm 0.003 \text{ \AA}^{-1}$, somewhat smaller than the value of $\tau = 2.15\pi\sqrt{B/\Phi_0} = 0.0105 \text{ \AA}^{-1}$ calculated from the flux quantization rule for an undistorted triangular lattice (Φ_0 is the flux quantum). Within experimental error, no such expansion of the average lattice spacing is observed for a larger θ . The slight expansion of the lattice for $\theta \approx 0^\circ$, together with the significant transverse broadening of four of the reflections, indicates the formation of defects that lead to an accumulation of vortices near twin planes.

Because of the poor longitudinal resolution of our instrument, we can only put a lower bound of ~ 3 lattice spacings on the translational correlation length. The instrumental resolution in the ϑ direction is much sharper ($\sim 0.2^\circ$), and rocking curves in the ϑ direction revealed an intrinsic width of $\Delta\vartheta \approx 1^\circ$ for the Bragg reflections, in agreement with previous measurements (9). The correlation length ξ^* of the vortex displacement field in the magnetic field direction is given approximately by $\xi^* = (\tau\Delta\vartheta)^{-1} \approx 6000 \text{ \AA}$ (10). The vortices are therefore significantly deflected from the field direction as they bend and follow the twin plane over some distance to gain advantage of the twin-plane pinning energy (11). In this model, the finite correlation length merely reflects the lack of long-range

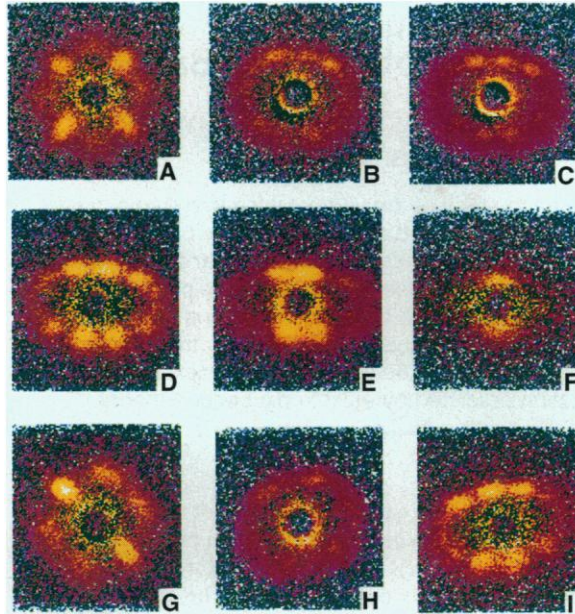


Fig. 3. Pseudocolor images of small-angle neutron scattering patterns taken with neutrons of wavelength 6 \AA at $T = 10 \text{ K}$. The window size is 0.023 by 0.023 \AA^{-2} . Bright central rings in some of the images are artifacts of the background subtraction. (A to F) $\chi = 0^\circ$, (G to I) $\chi = 9^\circ$. (A) $\theta = 0^\circ$, (B) $\theta = 40^\circ$, (C) $\theta = 50^\circ$, (D) $\theta = 60^\circ$, (E) $\theta = 70^\circ$, (F) $\theta = 80^\circ$, (G) $\theta = 5^\circ$, (H) $\theta = 30^\circ$, (I) $\theta = 60^\circ$.

order in the twin-plane position. The vortex line tension, which opposes this bending, leads to the formation of a single-domain pattern (Fig. 3G): The lowest elastic energy and maximum pinning energy of the vortex lattice are achieved if the orientation of one of the principal axes is given by the set of twin planes subtending the smaller angle α with respect to the magnetic field. The square pattern of Fig. 3A arises simply as a superposition of two orientations that are degenerate for $\chi = 0^\circ$.

The broadening of the ϑ rocking curves persists up to $\theta \sim 40^\circ$. However, for $\theta \geq 50^\circ$ the reflections become resolution-limited in all directions. These results are qualitatively consistent with high-temperature transport measurements (4) revealing a drop in the resistivity due to vortex motion when the magnetic field is applied within a “critical angle” with respect to the twin planes (12). It has been suggested (11) that vortex bending becomes energetically unfavorable above this critical angle; our neutron scattering data provide microscopic evidence for such behavior.

We now turn to the position of the Bragg reflections. In the “effective mass” model of an anisotropic superconductor, the reciprocal lattice vectors \vec{b}_1 and \vec{b}_2 of the vortex lattice, in terms of the coordinates \hat{y} and \hat{z} perpendicular to the magnetic field (Fig. 2), are given by (13)

$$\vec{b}_1 = \frac{\tau}{\sqrt{\epsilon(\theta)}} \begin{pmatrix} 0 \\ \epsilon(\theta) \end{pmatrix}$$

$$\vec{b}_2 = \frac{\tau}{\sqrt{\epsilon(\theta)}} \begin{pmatrix} \sin 60^\circ \\ \cos 60^\circ \epsilon(\theta) \end{pmatrix} \quad (1)$$

for $\chi = 0^\circ$. Here $\epsilon^2(\theta) = \epsilon^2 \sin^2 \theta + \cos^2 \theta$, and $\epsilon^2 = m_{ab}/m_c \ll 1$ is the effective mass

ratio, where ϵ is the penetration-depth anisotropy and m_{ab} and m_c are the effective masses in the ab plane and along the c axis, respectively. Inspection of the diffraction patterns of Fig. 3, B to E, reveals that although the distortion of the vortex lattice is consistent with Eq. 1, the orientation of the lattice does not follow the prediction of the effective mass model because no reflection with a zero \hat{y} component is observed. For a small θ , the orientation of the vortex lattice is determined by pinning interactions between vortices and twin planes. Therefore, we postulate that this relation remains true for a larger θ , which leads to a quandary. The correlation length of the displacement field along the magnetic field direction, for $\theta \geq 50^\circ$, is resolution-limited and therefore at least $\sim 2 \text{ \mu m}$. Hence, any bending of the vortex induced by the twin planes must be allowed to “heal” on a length scale shorter than the twin-plane spacing so that this bending does not cause a long-range displacement field reflecting the imperfect twin-plane periodicity. If, on the other hand, the vortex is assumed to be microscopically homogeneous, the pinning energy should not depend on the location of the intersection point between the vortex and the twin plane.

A length scale much shorter than the twin-plane spacing naturally arises in microscopic models of the vortex structure that also take the discreteness of the crystalline layer structure into account. In such models the vortex consists of “pancake” vortices in the ab plane separated by interplanar Josephson vortices. It has been argued (14) that the pinning forces experienced by the Josephson segments are reduced by a factor of $(\epsilon\xi/d)^3$ with respect to the force experienced by pancake vortices. For $\text{YBa}_2\text{Cu}_3\text{O}_7$, the in-plane coherence length is $\xi \sim 15 \text{ \AA}$ and the interlayer spacing is $d \sim 10 \text{ \AA}$, so that

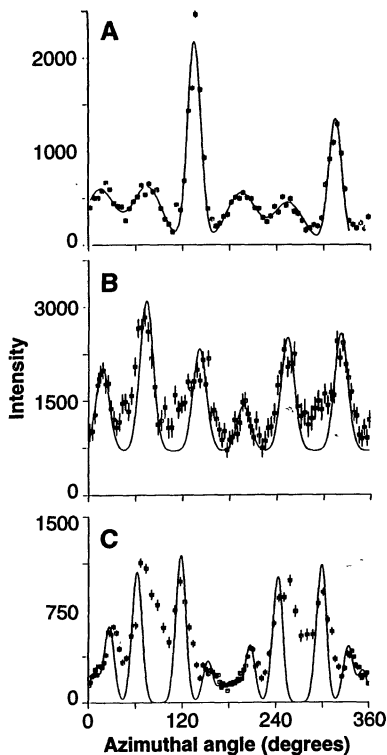


Fig. 4. Diffraction patterns for (A) $\chi = 9^\circ$, $\theta = 5^\circ$; (B) $\chi = 9^\circ$, $\theta = 30^\circ$; (C) $\chi = 0^\circ$, $\theta = 60^\circ$, radially averaged over an elliptical annulus of 15 to 20 pixels in width. The azimuthal angle is the angle subtended by a ray from the origin to the center of the annulus and the positive \hat{y} axis. (A) and (B) show six reflections corresponding to a single-domain vortex lattice. In (C) the Bragg condition is satisfied only for eight of the twelve reflections of the two-domain lattice. The solid lines show the peak positions predicted by Eq. 2. The relative peak heights carry no meaning (the intensity units are arbitrary).

we can neglect the pinning force on the interlayer segments and concentrate on the pinning forces on the pancakes. For $\epsilon^2 \ll 1$ and θ not too close to 90° , the projection of the lattice corresponding to the relation expressed in Eq. 1 onto the ab plane is an isotropic lattice with a lattice constant of $1.075 \sqrt{\Phi_0/B} / \sqrt{\cos\theta}$. The pinning energy of the pancake vortices is maximized when one of the principal axes of this lattice is parallel to the "picket fence" pattern of twin boundaries. Viewed along the field direction, the reciprocal lattice vectors of the rotated lattice in the two twin-plane domains are

$$\vec{b}_1 = \frac{\tau}{\sqrt{\cos\theta}} \begin{pmatrix} \pm \cos\chi \sin\phi \\ (\cos\theta \mp \sin\chi \sin\theta) \cos\phi \end{pmatrix}$$

$$\vec{b}_2 = \frac{\tau}{\sqrt{\cos\theta}} \begin{pmatrix} \pm \cos\chi \sin(\phi - 60^\circ) \\ (\cos\theta \cos(\phi - 60^\circ) \mp \sin\chi \sin\theta \sin(\phi - 60^\circ)) \end{pmatrix} \quad (2)$$

The high quality of our data allowed us to

carry out a detailed quantitative analysis of the peak positions. The radial peak positions were obtained from fits to sector averages and were found to be in quantitative agreement with Eq. 2 for $\theta \leq 60^\circ$. Three-dimensional corrections apply for $\theta \geq 70^\circ$. To obtain the angular peak positions, we averaged the data radially in an elliptical annulus of appropriate eccentricity. Figure 4 shows the typical results of this procedure, together with the predictions from Eq. 2. Except for the unexplained asymmetry of a few reflections, the observed peak positions are in substantial agreement with Eq. 2. This agreement validates our simple model and necessitates an essentially two-dimensional pinning mechanism.

Finally, we focus on the diffraction pattern for $\theta = 80^\circ$ (Fig. 3F), which is inconsistent with Eq. 2. In fact, the anisotropic London model (Eq. 1) predicts the position of these reflections correctly. A reorientation of the vortex lattice into the unique orientation predicted by anisotropic London theory is expected for a large θ because the elastic energy for rotations away from this orientation increases markedly for a large θ (15). Fits to high-quality diffraction patterns for B of 0.535 T, θ of 77° , and neutron wavelengths (λ) of 6 and 10 Å yield a value of $0.0061 \pm 0.0003 \text{ \AA}^{-1}$ for the radial peak position. The corresponding $\epsilon = 0.23 \pm 0.05$ is within the errors consistent with the values extracted from Bitter decoration patterns (16, 17).

For a large θ , the triangular vortex lattice is severely stretched in the direction perpendicular to both B and c and can be regarded as a collection of chains whose periodicities are locked. Anisotropic London theory predicts an attractive double well in the intervortex interaction along the chains for small fields, so that the vortices should penetrate as independent chains as the field is increased through the lower critical field H_{c1} . Such a vortex chain state has been observed in low-field Bitter decorations in $\text{YBa}_2\text{Cu}_3\text{O}_7$ (17). Some workers (18) have used the same theory to predict the persistence of this vortex chain state to much larger fields, due to an exponential softening of the vortex-lattice shear modulus corresponding to translations of the chains in the chain direction. In $\text{YBa}_2\text{Cu}_3\text{O}_7$ for $B = 0.5$ T, the chains are predicted to decouple for $\theta \geq 80^\circ$ (18), thus giving rise to a diffraction pattern consisting of just two reflections. The data represented in Fig. 3F confirm this prediction. By translating the detector with respect to the beam to probe a wider momentum range and taking diffraction patterns for different values of ϑ , we observed only broad and weak diffuse scattering around the remaining four reciprocal lattice vectors for fields of 0.1 and 0.5 T. The broadening of these Bragg peaks reflects

the loss of long-range order in the direction perpendicular to the chains.

In contrast to observations in other anisotropic superconductors (2), but in agreement with observations in $\text{YBa}_2\text{Cu}_3\text{O}_7$ at low fields (17), we therefore conclude that the mean field anisotropic London theory (13, 18) provides an adequate description of the structure and orientation of the vortex lattice in this material. However, we have also shown that pinning to correlated microstructural defects can obliterate this intrinsic behavior and lead to unexpected changes in morphology and orientation of the vortex lattice as a function of θ . It will be interesting to extend this investigation into a temperature and field range in which the melting of the flux-line lattice is expected to occur. For device applications, the strong response of the vortex lattice to the presence of twin planes, and the absence of any measurable influence of any other microstructural feature, makes the structural design and configuration of twin planes a promising approach to enhance the flux-trapping properties of these materials.

REFERENCES AND NOTES

1. D. J. Bishop *et al.*, *Science* **255**, 165 (1992).
2. H. F. Hess, C. A. Murray, J. V. Waszczak, *Phys. Rev. Lett.* **69**, 2138 (1992).
3. G. J. Dolan *et al.*, *ibid.* **62**, 827 (1989).
4. S. Fleshler *et al.*, *Phys. Rev. B* **47**, 14448 (1993); W. K. Kwok *et al.*, *Phys. Rev. Lett.* **69**, 3370 (1992); *ibid.* **64**, 966 (1990).
5. F. Doğan, unpublished data.
6. M. Sarikaya, R. Kikuchi, I. A. Aksay, *Physica C* **152**, 161 (1988); M. Sarikaya and E. A. Stern, *Phys. Rev. B* **37**, 9373 (1988).
7. The neutron scattering experiments were conducted on the NG-7 small-angle neutron scattering spectrometer at the Cold Neutron Research Facility of the National Institute of Standards and Technology. The crystal was attached to the cold finger of a closed-cycle helium refrigerator that was then mounted in an electromagnet. Most of our data were taken at $B = 0.5$ T with neutrons of wavelength 6 Å. After scattering from the sample, the neutrons were collected by an area detector ~ 15 m behind the sample. We used the standard "horizontal field" scattering geometry in which the magnetic field is nearly parallel to the neutron beam [G. Lippmann, J. Schelten, W. Schmatz, *Philos. Mag.* **33**, 475 (1976)]. In this geometry the Bragg condition (with typical scattering angles of $2\theta \sim 0.5^\circ$) is strictly met only for those reflections for which the angle between the magnetic field and the beam is set to be ϑ . In practice, however, the nonzero width of the reflections in the ϑ direction, resulting from vortex bending or resolution effects such as the angular divergence of the incoming beam and crystal mosaic, often allows the entire diffraction pattern to be taken while the beam is kept nominally parallel to B (that is, $\vartheta = 0$).
8. E. M. Forgan, *Physica B* **169**, 107 (1991); *et al.*, *Physica C* **185**, 247 (1991).
9. H. Yethiraj *et al.*, *Phys. Rev. Lett.* **70**, 857 (1993).
10. R. Labusch, *Phys. Status Solidi B* **69**, 539 (1975).
11. G. Blatter, J. Rhyner, V. M. Vinokur, *Phys. Rev. B* **43**, 7826 (1991).
12. The critical angle we observe ($\alpha_c \approx 30^\circ$ at $\theta = 45^\circ$) is substantially larger than the critical angles extracted from the transport measurements at comparable fields. Several corrections may apply (thermal wandering of the vortices around a twin plane, temperature dependence of the coherence

- length, and dynamic collective pinning effects), and a quantitative comparison between transport and neutron results will have to await further neutron measurements at elevated temperatures.
13. V. G. Kogan and L. J. Campbell, *Phys. Rev. Lett.* **62**, 1552 (1989); L. J. Campbell, M. M. Doria, V. G. Kogan, *Phys. Rev. B* **38**, 2439 (1988).
 14. G. Blatter and V. Geshkenbein, *Phys. Rev. B* **47**, 2725 (1993).
 15. Specifically, the deformed lattice corresponding to Eq. 2 can be approximately obtained from Eq. 1 by two orthogonal shear deformations, $\hat{u}_1 = \mu_1 y^2$ and $\hat{u}_2 = \mu_2 z^2$. The shear deformation \hat{u}_1 (with $\mu_1 = \sin 15^\circ / \sqrt{\cos \theta \epsilon(\theta)}$ for $\chi = 0^\circ$ and $\phi = 45^\circ$) vanishes between $\theta = 70^\circ$ and $\theta = 80^\circ$. The modulus for this shear mode (13) is $c_{66} = \Phi_0 B \epsilon^3(\theta) / (64\pi^2 \lambda_{ab}^2)$, where λ_{ab} is the penetration depth in the ab plane. The elastic energy $c_{66}(\mu_1/2)^2$ thus increases with θ as $\epsilon^2(\theta)/\cos(\theta)$, so that it is weakly dependent on θ for angles $\leq 70^\circ$, but increases sharply for a larger θ . This increase inevitably causes a reorientation in this range of angles. Clearly, the sharp reorientation implied in this argument is an artifact of the two-dimensional approximation we used in deriving Eq. 2. A refined model would smoothly interpolate between Eq. 1 and Eq. 2, as experimentally observed in our diffraction pattern for $\theta = 70^\circ$. A crude estimate of the pinning energy per pancake (or stack of pancakes) can be obtained from the morphology change we observe at $\alpha_c \sim 30^\circ$ ($\theta \sim 45^\circ$). On the assumption that for $\alpha < \alpha_c$ the vortices "kink" into

- segments of length $\sim D \cos \alpha$ pinned by the twin planes and unpinned sections of length $\sim D \sin \alpha$, and because the vortex line tension is $E_0 \epsilon(\theta) \ln[\lambda_{ab}/\xi \epsilon(\theta)]$, with $E_0 = \Phi_0 / 16\pi^2 \lambda_{ab}^2$ [R. A. Klemm and J. R. Clem, *Phys. Rev. B* **21**, 1868 (1980)], vortex bending becomes energetically unfavorable for $\tan \alpha_c \approx V_p / E_0$, where V_p is the pinning energy per unit length (logarithmic corrections of order unity depend on the detailed path taken by the vortices). According to the scenario discussed in the text, we expect V_p to be reduced by a factor $\sim d/D$ for $\alpha > \alpha_c$. Equating this relation to the elastic energy for the shear mode \hat{u}_1 yields $\theta \approx 80^\circ$ for the reorientation angle, consistent with our measurement.
16. G. J. Dolan, F. Holtzberg, C. Feild, T. R. Dinger, *Phys. Rev. Lett.* **62**, 2184 (1989).
 17. P. L. Gammel *et al.*, *ibid.* **68**, 3343 (1992).
 18. B. I. Ivlev and N. B. Kopnin, *Phys. Rev. B* **44**, 2747 (1991); ———, M. M. Salomaa, *ibid.* **43**, 2896 (1991).
 19. We thank J. Barker and C. Glinka for help with the small-angle neutron scattering instrument and software; V. Kiryukhin for assistance with the experiment; and D. J. Bishop, V. G. Kogan, and N. P. Ong for helpful discussions. Supported by the Advanced Research Projects Agency and the Air Force Office of Scientific Research (AFOSR) under grants AFOSR No. F49620-90-C-0079 and No. F49620-93-1-0259.

10 June 1993; accepted 11 August 1993

Anatomy of the Photodissociation Region in the Orion Bar

A. G. G. M. Tielens, M. M. Meixner, P. P. van der Werf, J. Bregman, J. A. Tauber, J. Stutzki, D. Rank

Much of the interstellar gas resides in photodissociation regions whose chemistry and energy balance is controlled by the flux of far-ultraviolet radiation upon them. These photons can ionize and dissociate molecules and heat the gas through the photoelectric effect working on dust grains. These regions have been extensively modeled theoretically, but detailed observational studies are few. Mapping of the prominent Orion Bar photodissociation region at wavelengths corresponding to the carbon-hydrogen stretching mode of polycyclic aromatic hydrocarbons, the 1-0 S(1) line of molecular hydrogen, and the $J = 1-0$ rotational line of carbon monoxide allows the penetration of the far-ultraviolet radiation into the cloud to be traced. The results strongly support the theoretical models and show conclusively that the incident far-ultraviolet radiation field, not shocks as has sometimes been proposed, is responsible for the emission in the Orion Bar.

Photodissociation regions (PDRs), sometimes called photodominated regions, are regions in which far-ultraviolet (FUV) photons with energies less than the hydrogen ionization limit dominate the energy bal-

ance or chemical composition of the interstellar gas (1). PDRs are associated with HII regions, reflection nebulae, bright-rim clouds, planetary nebulae, and normal and active galactic nuclei (2). Indeed, most of the neutral atomic and molecular gas in the galaxy is in regions where penetrating FUV photons play an important role.

Although much theoretical effort has been expended on the development of models for the interaction of FUV photons with interstellar gas, little direct observational data on this interaction is presently available. Photons with energies above 13.6 eV can ionize H and, in a natural way, lead to ionized gas regions with temperatures of 10^4 K, which emit predominantly in the visible and UV. Hence, observation-

al studies of H^+ regions have a long and distinguished history in astronomy. In contrast, neutral atomic and molecular gas cool down to much lower temperatures ($< 10^3$ K) and in consequence emit essentially all of their energy at infrared (IR) and submillimeter wavelengths. Because of the high thermal background associated with ground-based telescopes, observations in the IR require special techniques, and very extended regions of low surface brightness (which encompass most of the galactic gas) are impossible to study.

We circumvented this problem by studying a dense and compact region near a luminous O star, which hence has a high surface brightness. Recent advances in IR detector technology now allow efficient mapping of such objects in the rovibrational lines of H_2 and the vibrational transitions of polycyclic aromatic hydrocarbon molecules (PAHs). Moreover, present telescope arrays operating at millimeter wavelength can spatially resolve these regions in the transition of the most abundant carbon-bearing molecule, CO. Hence, a combination of these techniques permits a direct observational study of the detailed interaction of FUV photons with atomic and molecular gas.

Theoretical studies (1) show that for a bright PDR, as considered here, the chemical structure is mainly determined by the penetration of FUV photons and hence by the dust extinction. A nearby O star creates a surface layer of predominantly neutral gas (mostly neutral H along with neutral O and C^+ and Si^+) that separates the ionized gas from the surrounding prenatal molecular cloud. At an optical depth of about $A_v = 2$ magnitudes (mag), the dissociating photons have been sufficiently attenuated, and neutral H transforms into H_2 . Similarly, at $A_v \approx 4$ mag, the carbon balance shifts from C^+ to neutral C and CO.

The penetrating FUV photons also dominate the energy balance of the gas. Near the surface ($A_v < 4$ mag), heating occurs primarily through the photoelectric effect on dust grains and PAH molecules. The gas cools predominantly through atomic fine-structure lines: notably, [OI] 63 μm and [CII] 158 μm (neutral O and singly ionized C, which have lines at wavelengths, λ , of 63 and 158 μm , respectively; the brackets indicate a "forbidden" transition). The gas in this zone is fairly warm, ≈ 500 K, much warmer than the dust (≈ 75 K). Because of dust attenuation, photoelectric heating becomes less important deeper in the PDR ($A_v > 4$ mag), and collisions of gas species with warm dust grains, heated by penetrating visible and IR photons, take over as the dominant heating source. The gas cools efficiently through CO rotational lines. As a result, the gas is now slightly cooler (≈ 50

A. G. G. M. Tielens and J. Bregman, MS 245-3 NASA Ames Research Center, Moffett Field, CA 94035-1000.

M. M. Meixner, Radioastronomy Laboratory, University of California, Berkeley, CA 94720.

P. P. van der Werf, Max Planck Institut für Extraterrestrische Physik, Giessenbach Strasse, D-8046 Garching bei München, Germany.

J. A. Tauber, Radioastronomy Laboratory, University of California, Berkeley, CA 94720, and ESA Astrophysics Division, ESTEC, P.O. Box 299, NL-2200 AG Noordwijk, the Netherlands.

J. Stutzki, I. Physikalisches Institut, Universität Köln, Zùlpicherstrasse 77, W-5000 Köln 41, Germany.

D. Rank, Lick Observatories, University of California, Santa Cruz, CA 95060.